Retrospective SPECT/CT Dosimetry Following Transarterial Radioembolization

Briana C. Thompson (brthomps@wakehealth.edu)
Wake Forest University School of Medicine https://orcid.org/0000-0002-4691-3628
William A. Dezarn
Wake Forest Baptist Medical Center

Original research

Keywords: Y90 Bremsstrahlung SPECT/CT, Radioembolization, dose distribution, imaged based dosimetry

Posted Date: August 24th, 2020

DOI: https://doi.org/10.21203/rs.3.rs-61528/v1

Abstract

Background: Transarterial Radioembolization (TARE) effectively treats unresectable primary and metastatic liver tumors through local injection of Yttrium-90 (^{90}Y) beta particle emitting microspheres. These microspheres implant around the tumor, damaging tumorous cells while sparing healthy liver tissue. Current dosimetry models are highly simplistic and based patient characteristics such as body surface area and fail to consider many important factors. There is a large need for an imaged based dosimetry post-TARE which would improve treatment safety and efficacy. Current post-TARE imaging is ^{90}Y bremsstrahlung SPECT/CT and we study the use of these images for post-TARE dosimetry.

Methods: Retrospective image review of 10 patients having a Philips Healthcare^{TM} SPECT/CT following TARE SIR-Spheres® implantation. Emission series with attenuation correction were resampled to 3mm resolution and used to create image based dose distributions. Dose distributions and analysis were performed in MIM Software SurePlan^{TM} utilizing SurePlan^{TM} Local Deposition Method (LDM) and our own dose convolution method (WFBH). We sought to implement a patient specific background subtraction technique prior to dose calculation to make these noisy bremsstrahlung SPECT images suitable for post-TARE dosimetry calculations.

Results: On average the percentage of mean background counts to maximum count in the image across all patients was 9.4 ± 4.9% with a maximum of 17.6% and minimum of 2.3%. Absolute dose increased and profile line width decreased as background subtraction value increased. The average value of the LDM and WFBH dose methods were statistically the same. As background subtraction value increased, we found the DVH curves to become unrealistic and distorted.

Conclusion: Background subtraction on bremsstrahlung SPECT image had a large effect on post-TARE dosimetry. The background contour we defined provides a systematic estimate to the activity background that accounts for the scanner and patient conditions at the time of the image study and is easily implemented using commercially available software. We found using the mean count in the background contour as a constant subtraction across the entire image gave the most realistic dose distributions. Comparison of dosimetry from background subtracted SPECT images to image based dosimetry obtained via ^{90}Y PET images will be the subject of our next analysis.

Background

Transarterial Radioembolization (TARE) uses beta particle emitting microspheres to treat unrespectable primary and metastatic liver tumors. These Yttrium-90 (^{90}Y) containing spheres are injected locally around the tumor(s) where they will become lodged in the tumor microvasculature delivering 95% of the radiation dose within 11 days due to its half-life of 64.2 hours[1]. Mean range for radiation delivery is 2.5 mm with a maximum penetration depth of 11 mm, allowing for local irradiation of tumor cells while sparing healthy liver tissue[2, 3]. During pretreatment planning, Technetium-99m macroaggregated albumin particles (^{99m}Tc-MAA) are used to mimic the dispersion of microspheres upon treatment and are

considered an acceptable surrogate for the basis of dosimetry calculations [2, 4–6]. Although they act as an acceptable prediction for microsphere distribution there is still a need for post-TARE emission imaging for validation of microsphere placement, especially for patient safety [1, 7–10].

Upon completion of TARE treatment, a ^{90}Y bremsstrahlung single-photon emission computed tomography (SPECT) imaging study is acquired to identify any extrahepatic microsphere deposition [2, 3, 11]. Historically, these images are only used only for qualitative information due to their noisy nature but some groups have shown their potential in quantitative imaging upon extra image processing[2, 12, 13]. Many challenges are present using these ^{90}Y bremsstrahlung SPECT images quantitatively. One is due to the continuous bremsstrahlung spectrum with a wide photon energy range of 0-2.3MeV[1, 14]. Another is a lack of distinct photopeaks that are routinely used in SPECT imaging[1, 12, 14]. The high-energy photons can penetrate through the collimator septa[1, 14]. Just these few concerns lead to very noisy, low resolution, images.

There is a general consensus on the benefits of accurate image based post-TARE dosimetry among researchers in the field but a lack of information on best practices using commercially available software makes implementation across intuitions difficult[1, 2, 4, 15]. Recently there have been advancements in understanding the promising nature of post-TARE ^{90}Y positron emission tomography (PET) image based dosimetry, however it needs to be noted that not all institutions may have the feasibility to obtain ^{90}Y PET images post-TARE. At such locations, it is still imperative to perform post-TARE dosimetry thus there is still a need to better understand how to best use bremsstrahlung SPECT images for accurate dosimetry. In this study, we sought to create a way to address background noise on these post-TARE SPECT images on an easily implemented patient specific basis and determine background subtraction effects on resulting dose distributions.

This study, to our knowledge, is the first to look at a systematic estimate to the activity background that accounts for the scanner and patient conditions at the time of the image study and its effects on post-TARE SPECT based dosimetry.

Methods

Through an IRB approved retrospective study we created post-TARE image based dose distributions for 10 patients treated with SirTex SirSpheres™ ^{90}Y microspheres for hepatic malignancies at Wake Forest Baptist Medical Center. Each patient had a bremsstrahlung SPECT/CT (parameters shown in Table 1) utilizing a Philips Healthcare™ scanner following SIR-Spheres® implantation.

Table 1
Post-TARE SPECT/CT imaging parameters

Imaging Parameter	^{90}Y bremsstrahlung post-TARE SPECT
Energy window	328.04 KeV – 400 .94 KeV
Collimator type	parallel
Spatial resolution	3.4 mm
Scan arc	360°
Number of frames in rotation	64
Type of detector motion	Step and shoot
Field of view dimensions	597 mm x 597 mm
Voxel size	4.664 mm x 4.664 mm x 4.664 mm

The SPECT images were attenuation corrected with the CT data, which was the only scanner correction. Using MIM Software SurePlan™ (MIM Software Inc., Cleveland, OH) the SPECT images were resampled to 3 mm resolution and contours were drawn for organs of interest based on the registered CT image. Dose distributions, as shown in Fig. 1, were created based on these bremsstrahlung SPECT images using SurePlan™ Local Deposition Method (LDM) and our own dose convolution method (WFBH), both applied at the voxel level. Through the process of creating dose distributions, the emission image was scaled based on actual delivered activity at the time of treatment. Within the LDM model, the normalization and dose calculation is based on counts found within the liver contour. We expanded this contour by 20 mm on all sides prior to any normalization in order to account for potential movement during imaging as well as if activity is located close to the edge of the liver. For WFBH, the normalization is based on the total counts found in the body contour. Table 2 shows the patient characteristics and treatment details of those included for this analysis.

Table 2
Patient characteristics who were included in this study

Patient no.	Sex	Lung Shunt	Treated Volume	Liver (cm^3)	Tumor (cm^3)	SMAC Activity (GBq)	Activity Delivered (GBq)
1	Male	4.39%	Rt Lobe	1715.5	129.5	0.97	1.040
2	Female	2.42%	Rt Lobe	2065.7	521.4	1.07	1.069
3	Female	3.32%	Seg 4	2109.5	73.4	0.25	0.252
4	Male	6.47%	Rt Lobe	1839.8	73.0	1.00	1.051
5	Female	1.10%	Rt Lobe	1880.3	478.5	1.37	1.391
6	Female	5.11%	Rt Lobe	1756.8	204.6	1.60	1.698
7	Male	3.59%	Rt Lobe	2212.9	304.2	0.97	1.006
8	Female	2.79%	Rt Lobe	1990.7	139.0	0.90	0.932
9	Female	2.41%	Rt Lobe	2741.2	690.7	1.25	1.136
10	Female	1.46%	Lt Lobe	1972.8	218.6	0.90	0.947

The main goal of this study was to understand how the noise within these bremsstrahlung SPECT images affects the resultant image based dose distributions. In order to try get a handle on eliminating the background noise in the image while not eliminating true counts, we created a background contour defined to be the whole body contour minus the liver and lungs expanded by 20 mm. This contour was originally created on the CT image and transferred to the emission series where its statistics were recorded. Figure 2 shows an example of this contoured area, shaded in blue. In addition to dose distributions created using LDM and WFBH dose calculation methods on the original SPECT images, we created dose distributions after a constant background subtraction on the emission image was performed. We wrote an extension in Java (Oracle corporation et al., Redwood City, CA, USA) to run in MIM (see supplementary material for code) in order to easily subtract background on a patient by patient case. The extension prompts you to enter a background value (in counts) which will be subtracted from the entire emission image. If a given voxel value becomes negative due to the subtraction, it will set to zero (0). We defined the following shorthand for the various corrected images we created based on the different background contour statistics being subtracted: Bkgrd = mean counts in background contour subtracted from all voxels, Bkgrd + SD = Bkgrd plus one standard deviation subtracted, Bkgrd + 2SD = Bkgrd plus two standard deviations subtracted. Table 3 shows a summary of the background contour statistics for the patient's in this study. Once we performed all three background subtractions on the original emission image, we then created dose distributions using LDM and WFBH methods for each corrected image, thus in total, for each patient we had 8 dose distributions. Four dose distributions were created using LDM, one with the resampled image and three others from the background subtraction levels. Similarly, four dose distributions were created using WFBH method.

Dose volume histogram (DVH) curves and dose profiles were used to compare the different dose distributions obtained in this study. Dose profiles were created by defining the max dose point, obtained via WFBH Bkgrd method, and drawing a sagittal line passing through this point. This line was transferred to all dose images for consistency in the spatial dimension for the line profile comparisons.

Results

Figure 3 demonstrates the visual effects of our background subtraction technique showing the effectiveness of our technique. However, the question then becomes at what point are true counts being artificially subtracted out of the image as we increase the background value. *Table 3* allows us to better understand the magnitude of these background. The background values range from 9.4% ± 4.9 % to 23.5% ± 11.6% of the max count value in the image, showing we are subtracting a substantial count value compared to the largest value in the image. Additionally, *Table 3* shows that although most counts within this background contour are small, you can see that there are still large values within this area, just furthering the point that this background subtraction is necessary considering that in theory, there should be no counts found within this contour. By subtracting these low count values uniformly across the image we are decreasing the amount of noise and low dose in the image.

Table 3 Statistics for the background contour for each patient based on SPECT counts

Patient no.	Mean background count	Background count max	Background count standard deviation
1	5.0	76.8	4.8
2	5.1	27.4	3.6
3	1.6	15.4	1.5
4	6.5	58.3	5.6
5	7.7	47.0	5.8
6	3.9	20.9	2.7
7	6.6	40.1	5.0
8	4.7	38.0	4.1
9	6.5	32.2	4.3
10	5.1	85.0	3.8

As expected, *Table 4* shows that as the subtracted background value increases, the max dose value increases for both dose calculation methods. This trend further demonstrates that a statistically defined background subtraction is needed. No background correction can predict too low of a dose delivered while too high of a background subtraction will predict too high of a dose delivered.

Table 4 Effect of background subtraction on maximum dose value

	Ratio of max dose values between background subtracted images and original images					
	WFBH Bkgrd: WFBH	WFBH Bkgrd + SD: WFBH	WFBH Bkgrd + 2SD: WFBH	LDM Bkgrd: LDM	LDM Bkgrd + SD: LDM	LDM Bkgrd + 2SD: LDM
Average	6.692	10.503	15.864	4.805	7.516	11.270
Standard Deviation	2.351	4.056	7.483	2.012	3.439	6.005

Ratio of max dose value obtained after background subtraction compared to its respective original image max dose value averaged over all patients

The dose line profiles in *Figure 4a* demonstrate that absolute dose is effected by background subtraction, the maximum dose increases as the background subtraction value increases. When the dose line profiles are normalized to the maximum point in each respective method, we see that dose distributions are not spatially being effected for a given background level (*Figure 4b*). Also note in *Figure 4b* the low dose region shrinking as the background subtraction value increases. This demonstrates the potential of removing low dose delivered regions that could important to consider in future patient care. Through these dose profiles we see an agreement between LDM and WFBH dose calculation methods and *Table 5* shows the agreement of the resulting maximum dose values. LDM yielded higher maximum dose values on average without background consideration but upon background subtraction the two methods give comparable ratios.

Table 5 Comparison of LDM and WFBH maximum dose values

	Ratio of max dose values obtain via LDM and WFBH methods			
	LDM: WFBH	LDM Bkgrd: WFBH Bkgrd	LDM Bkgrd + SD: WFBH Bkgrd + SD	LDM Bkgrd + 2SD: WFBH Bkgrd + 2SD
Average	1.378	0.970	0.967	0.966
Standard Deviation	0.205	0.106	0.105	0.106

Ratio of max dose values obtained comparing LDM to WFBH dose calculation methods, averaged over all patients

Figure 5 shows representative DVH curves for the listed liver dose distributions. We found that DVH curves for WFBH and LDM methods were not statistically different in 39 out of 44 curves through two

tailed p-values (statistical significance deemed to be less than 0.05). In these 5 curves that were deemed statistically different, 3 were from the same patient and were for the resulting DVH curves after each background subtraction value. *Figure 6* shows the DVH curves for this patient and as we see the LDM method is shifted below the WFBH method in these three cases. The other 2 statistically different curves were for just one set of curves in each patient. Across all three patients their treatment area is right at the edge of the liver contour.

In *Figure 5-7* WFBH Bkgrd and LDM Bkgrd show an expected shape change for DVH curves due to the decrease in low dose and increase in high dose as well as healthy tissue sparing. *Figure* 7 shows DVH curves for the treated region, defined to be the region that is up to 20% of the max activity. These curves demonstrate better dose coverage with Bkgrd subtraction value compared to no correction. At the same time, Bkgrd + SD and Bkgrd + 2SD DVH curves show that these background values are unphysically skewing the delivered dose distribution to less coverage at low dose values than no background correction hence an unphysical altering of dose distribution at these levels. With Bkgrd subtraction level we do not see this effect and it is deemed the largest value we can subtract without creating unphysical changes in the DVH curves.

Discussion

Although ^{90}Y PET imaging is thought to be superior for post-TARE dosimetric needs due to improved spatial resolution[16–18], it cannot be assumed that all institutions performing these treatments have access to such imaging modalities. Therefore, a better understanding of the dosimetric outcomes based on bremsstrahlung SPECT images is still necessary. By utilizing commercially available software in this study we are also enhancing the ability for post-TARE image based dosimetry calculations to become standard practice, something that is highly lacking in this field currently due to the imaging complexities associated with ^{90}Y.

We explored one methodology of trying to eliminate false counts in the emission scan prior to dosimetry calculations. In theory, within the background contour we created, there should not be activity present so we used this area to help us identify on average what portion of counts within our organs of interest are true and which are false. Our rationale of expanding the liver and lung contour 2cm was to try to account for the potential breathing motion of the patient during imaging.

As the background value increased in magnitude, we found the overall max dose of the resulting dose distributions to increased, which was expected because absorbed dose within a voxel is calculated via the following equation:

$$D_{voxel} = \frac{A(1 - LSF)T_{1/2}E_{avg}C_{voxel}}{\Delta V\, \rho \ln(2) C_{total}}$$

where A =activity, LSF = lung shunt fraction, $T_{1/2}$ = ^{90}Y half-life, E_{avg} = average β-particle energy per disintegration (0.935 MeV), C_{voxel} = counts within voxel, ΔV = voxel volume, ρ = tissue density, and C_{total} = total counts within the patient[15]. The calculated dose in a given voxel is the voxel value divided by the total counts multiplied by a constant. So as the background subtraction level increases, the count total decreases, which is in the denominator, thus causing the calculated dose value to increase.

An assumption of the LDM model is that all the energy from β-particle decay is locally within the same voxel[15]. WFBH method uses a 5x5x5 scattering kernel to consider the effects on neighboring voxels. However, through our analysis in this study it appears this does not make a considerable difference in resulting dose distributions when using ^{90}Y Bremsstrahlung SPECT images. This is likely due to the mean range of β-particles in tissue being 2.5mm and using a resampled voxel size of 3mm in our emission scan.

Overall, either LDM or a convolution method like WFBH applied at the voxel level with the mean counts in the background contour subtracted uniformly across the image gives the most realistic post-TARE dosimetry based on ^{90}Y bremsstrahlung SPECT images. Further work needs to address how these models with mean background subtraction compare to dose distributions based on ^{90}Y PET images to further validate accuracy.

Conclusion

Image processing, such as background subtraction, has a large effect on post-TARE SPECT dosimetry. Both LDM and WFBH convolution method applied at the voxel level with constant background subtraction appear to give reasonable post-TARE dosimetry based on DVH curves and dose profiles. We defined easy to implement steps for image based on ^{90}Y bremsstrahlung SPECT post-TARE images despite their inherent noisy nature. Our recommended protocol for post-TARE image based dosimetry using bremsstrahlung SPECT imaging is as follows:

1. Resample SPECT image to 3mm resolution
2. Contour the whole body, liver and lungs on CT
3. Expand liver and lung contours by 20mm
4. Subtract the union of expanded liver and lung contour from whole body
5. Transfer contour to resampled SPECT image
6. Record the mean counts within this new background contour
7. Run background subtraction extension (code found in supplemental information) by selecting the SPECT image, input mean background count value and save new background subtracted image
8. Use a voxel based dosimetry method on 3mm resampled background subtracted SPECT image

Our goal is to educate and emphasize the importance of post-TARE image based dosimetry in order to move the field towards making background subtracted SPECT images a standard protocol in order to

improve patient treatment dosimetry and outcomes.

List Of Abbreviations

TARE: Transarterial Radioembolization

^{90}Y: Yttrium-90

SPECT: single-photon emission computed tomography

PET: positron emission tomography

SPECT/CT: single-photon emission computed tomography/computed tomography

CT: computed tomography

LDM: SurePlan^{TM} Local Deposition Method

WFBH: our dose convolution method

DVH: dose volume histogram

Declarations

Ethics approval: This research study was conducted retrospectively from data obtained for clinical purposes. We consulted extensively with the IRB of WFBH who determined that our study did not need ethical approval. An IRB official waiver of ethical approval was granted from the IRB of WFBH.

Consent to participate: Informed consent was waived by the IRB of WFBH.

Consent for publication: Informed consent was waived by the IRB of WFBH.

Availability of data and material: The datasets generated during and/or analyzed during the current study are available from the corresponding author on reasonable request.

Competing interests: BCT declares no conflict of or competing interests. WAD serves as an advisory board consultant for Sirtex Medical.

Funding: Not applicable

Authors' contributions: Both authors contributed to the conception, design and analysis of the study. Data collection was performed by BCT. First draft of the manuscript was written by BCT and WAD commented and edited on each version of the manuscript. Both authors read and approved the final manuscript.

Acknowledgements: We would like to thank Dorsey Faught and Will Cork with MIM Software™ for their help in creating workflows within their software to automate the dosimetry calculation and analysis process.

References

1. Tafti BA, Padia SA. Dosimetry of Y-90 Microspheres Utilizing Tc-99m SPECT and Y-90 PET. Semin Nucl Med. 2019;49:211–7.
2. Dezarn WA, Cessna JT, DeWerd LA, Feng W, Gates VL, Halama J, et al. Recommendations of the American Association of Physicists in Medicine on dosimetry, imaging, and quality assurance procedures for 90Y microsphere brachytherapy in the treatment of hepatic malignancies. Med Phys. 2011;38:4824–45.
3. Kennedy A, Nag S, Salem R, Murthy R, McEwan AJ, Nutting C, et al. Recommendations for Radioembolization of Hepatic Malignancies Using Yttrium-90 Microsphere Brachytherapy: A Consensus Panel Report from the Radioembolization Brachytherapy Oncology Consortium. Int J Radiat Oncol. 2007;68:13–23.
4. Garin E, Rolland Y, Laffont S, Edeline J. Clinical impact of 99mTc-MAA SPECT/CT-based dosimetry in the radioembolization of liver malignancies with 90Y-loaded microspheres. Eur J Nucl Med Mol Imaging. 2016;43:559–75.
5. Song YS, Paeng JC, Kim H-C, Chung JW, Cheon GJ, Chung J-K, et al. PET/CT-Based Dosimetry in 90Y-Microsphere Selective Internal Radiation Therapy: Single Cohort Comparison With Pretreatment Planning on 99mTc-MAA Imaging and Correlation With Treatment Efficacy. Medicine (Baltimore) [Internet]. 2015 [cited 2020 Jul 23];94.
6. Kafrouni M, Allimant C, Fourcade M, Vauclin S, Guiu B, Mariano-Goulart D, et al. Analysis of differences between 99mTc-MAA SPECT- and 90Y-microsphere PET-based dosimetry for hepatocellular carcinoma selective internal radiation therapy. EJNMMI Res. 2019;9:62.
7. Scott NP, McGowan DR. Optimising quantitative 90Y PET imaging: an investigation into the effects of scan length and Bayesian penalised likelihood reconstruction. EJNMMI Res. 2019;9:40.
8. Wondergem M, Smits MLJ, Elschot M, de Jong HWAM, Verkooijen HM, van den Bosch MAAJ, et al. 99mTc-macroaggregated albumin poorly predicts the intrahepatic distribution of 90Y resin microspheres in hepatic radioembolization. J Nucl Med Off Publ Soc Nucl Med. 2013;54:1294–301.
9. Jiang M, Fischman A, Nowakowski FS. Segmental Perfusion Differences on Paired Tc-99m Macroaggregated Albumin (MAA) Hepatic Perfusion Imaging and Yttrium-90 (Y-90) Bremsstrahlung Imaging Studies in SIR-Sphere Radioembolization: Associations with Angiography. J Nucl Med Radiat Ther [Internet]. 2012 [cited 2020 Jun 25];03.
10. Knešaurek K, Machac J, Muzinic M, DaCosta M, Zhang Z, Heiba S. Quantitative Comparison of Yttrium-90 (90 Y)-Microspheres and Technetium-99m (99m Tc)-Macroaggregated Albumin SPECT Images for Planning 90 Y Therapy of Liver Cancer. Technol Cancer Res Treat. SAGE Publications Inc; 2010;9:253–61.

11. Rowley LM, Bradley KM, Boardman P, Hallam A, McGowan DR. Optimization of Image Reconstruction for 90Y Selective Internal Radiotherapy on a Lutetium Yttrium Orthosilicate PET/CT System Using a Bayesian Penalized Likelihood Reconstruction Algorithm. J Nucl Med. 2017;58:658–64.
12. Porter CA, Bradley KM, Hippeläinen ET, Walker MD, McGowan DR. Phantom and clinical evaluation of the effect of full Monte Carlo collimator modelling in post-SIRT yttrium-90 Bremsstrahlung SPECT imaging. EJNMMI Res. 2018;8:7.
13. Rong X, Du Y, Ljungberg M, Rault E, Vandenberghe S, Frey EC. Development and evaluation of an improved quantitative 90Y bremsstrahlung SPECT method. Med Phys. 2012;39:2346–58.
14. Elschot M, Vermolen BJ, Lam MGEH, Keizer B de, Bosch MAAJ van den, Jong HWAM de. Quantitative Comparison of PET and Bremsstrahlung SPECT for Imaging the In Vivo Yttrium-90 Microsphere Distribution after Liver Radioembolization. PLOS ONE. Public Library of Science; 2013;8:e55742.
15. Potrebko PS, Shridhar R, Biagioli MC, Sensakovic WF, Andl G, Poleszczuk J, et al. SPECT/CT image-based dosimetry for Yttrium-90 radionuclide therapy: Application to treatment response. J Appl Clin Med Phys. 2018;19:435–43.
16. Willowson K, Forwood N, Jakoby BW, Smith AM, Bailey DL. Quantitative (90)Y image reconstruction in PET. Med Phys. 2012;39:7153–7159.
17. D'Arienzo M, Chiaramida P, Chiacchiararelli L, Coniglio A, Cianni R, Salvatori R, et al. 90Y PET-based dosimetry after selective internal radiotherapy treatments. Nucl Med Commun. 2012;33:633–40.
18. Lhommel R, van Elmbt L, Goffette P, Van den Eynde M, Jamar F, Pauwels S, et al. Feasibility of 90Y TOF PET-based dosimetry in liver metastasis therapy using SIR-Spheres. Eur J Nucl Med Mol Imaging. 2010;37:1654–62.

Figures

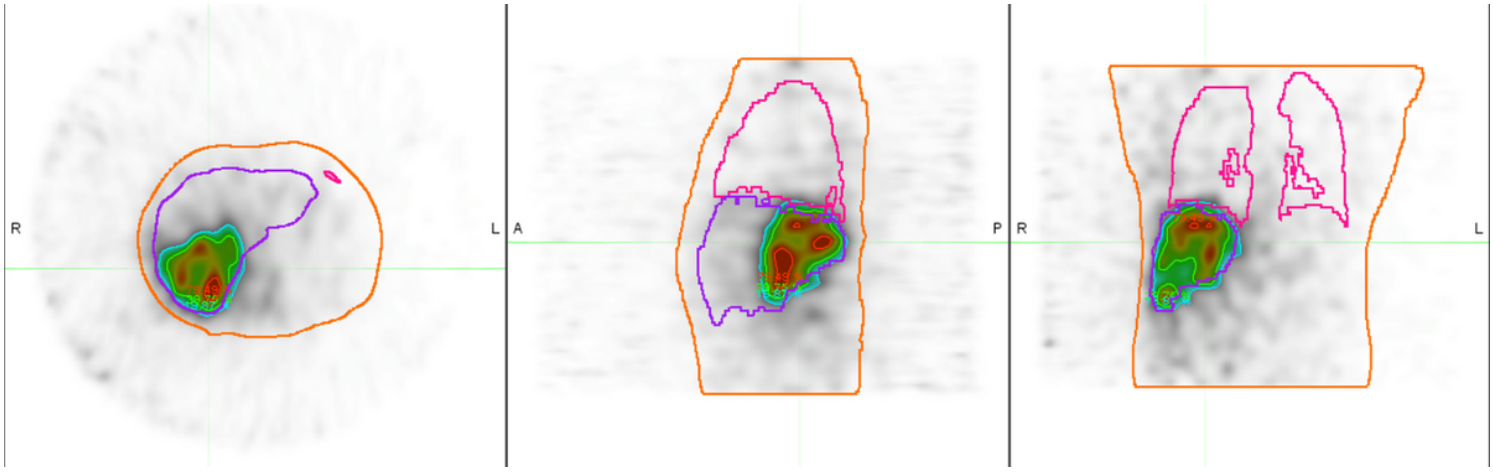

Figure 1

Dose distribution example Representative SPECT image showing WFBH +Bkrgd dose method. The whole body is contoured in orange, liver in purple and lungs in pink. Red denotes 100 Gy, green is 50 Gy and blue

is 25 Gy. Note the noisy nature of the image.

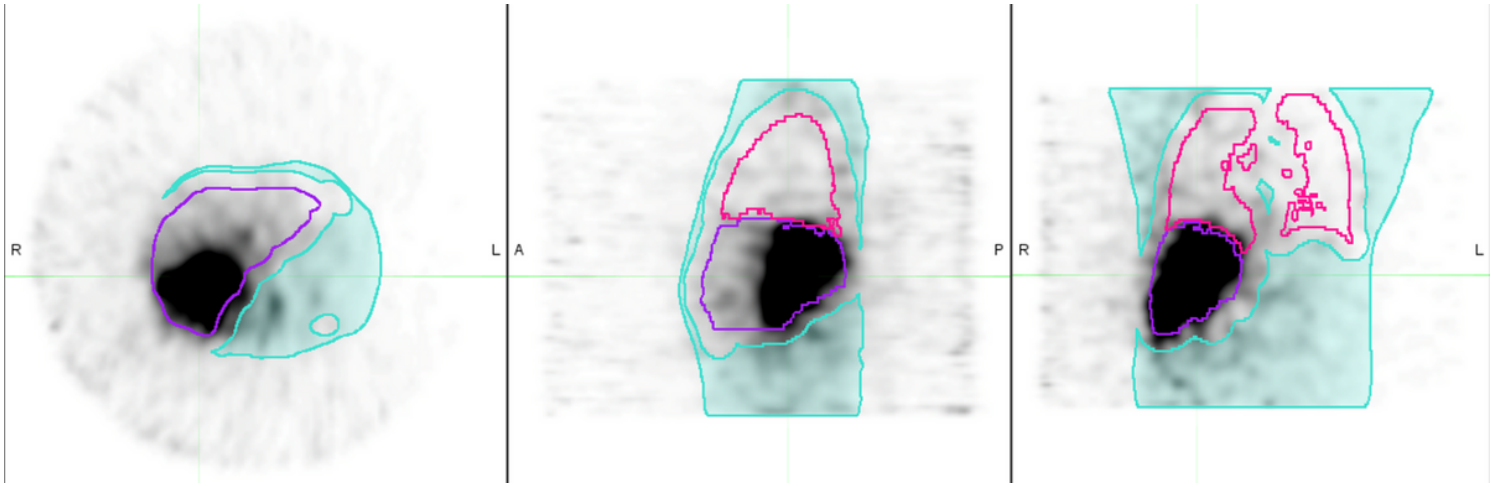

Figure 2

Background contour example Representative SPECT image showing the background contour in blue, liver in purple and lungs in pink.

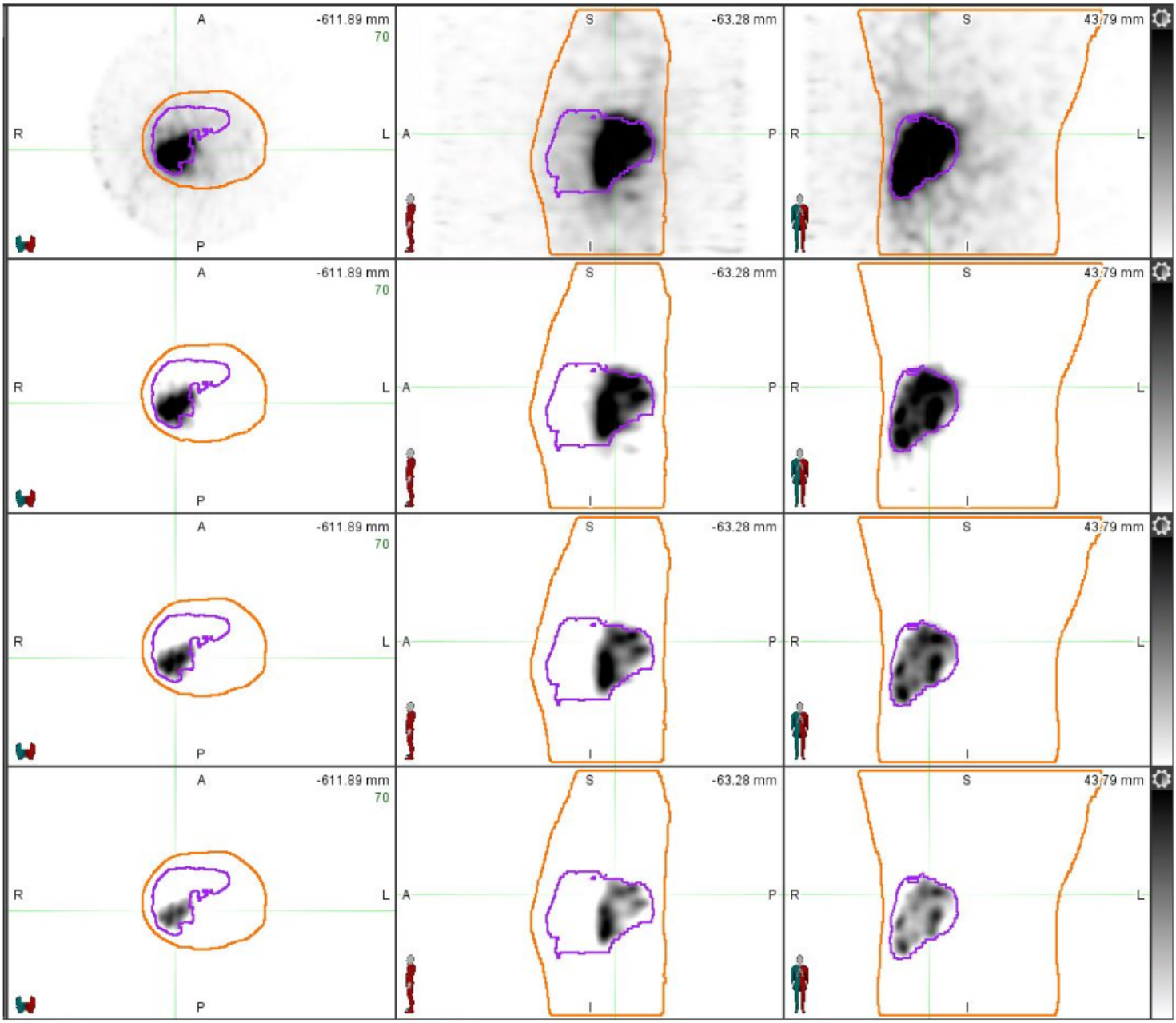

Figure 3

Visual representation of background subtraction on image Representative images showing for the same patient, the effects of our background subtraction technique. Each row represents a different subtraction value starting from the top row having no subtraction, second row mean value subtraction, third being mean + SD and last row is mean + 2SD.

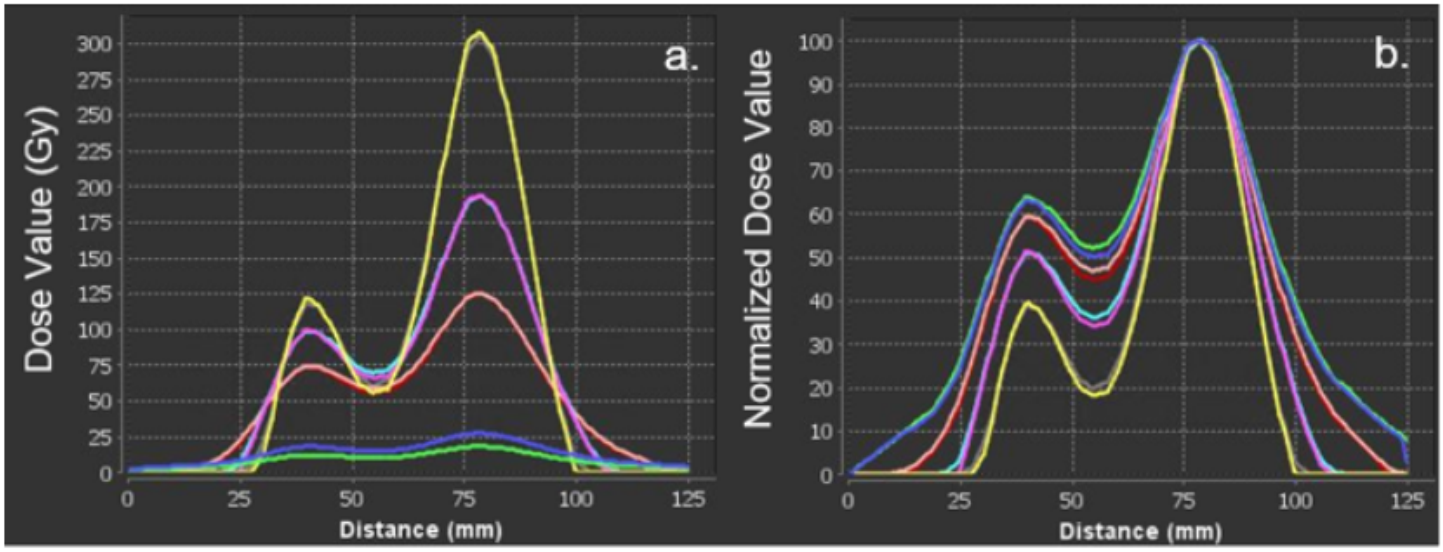

Figure 4

Representative dose profile Sagittal dose profile through the max dose point. Fig 4a shows the dose value in Gy on the y-axis and an arbitrary location on the x-axis. Fig 4b shows the normalized dose value on the y-axis and an arbitrary location on the x-axis. Dark blue line represents WFBH method, green is LDM method, peach is WFBH Bkgrd, red is LDM Bkgrd, magenta is WFBH Bkgrd + SD, light blue is LDM Bkgrd + SD, yellow is WFBH Bkgrd + 2SD and grey is LDM Bkgrd + 2SD.

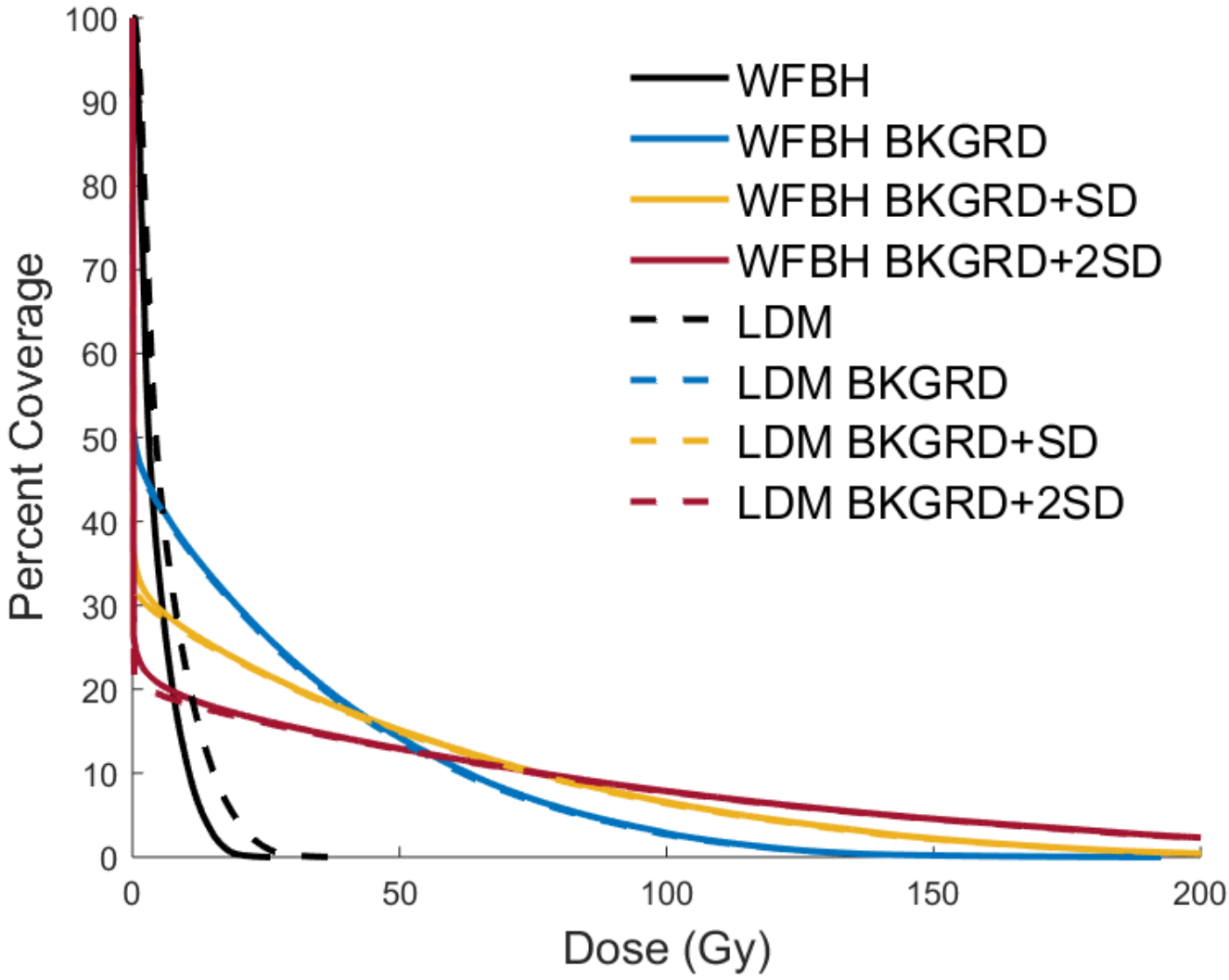

Figure 5

Liver DVH curves Showing the effect background subtraction has on the DVH curves for both dose calculation methods. We see dose method has little effect while background subtraction value has large effect.

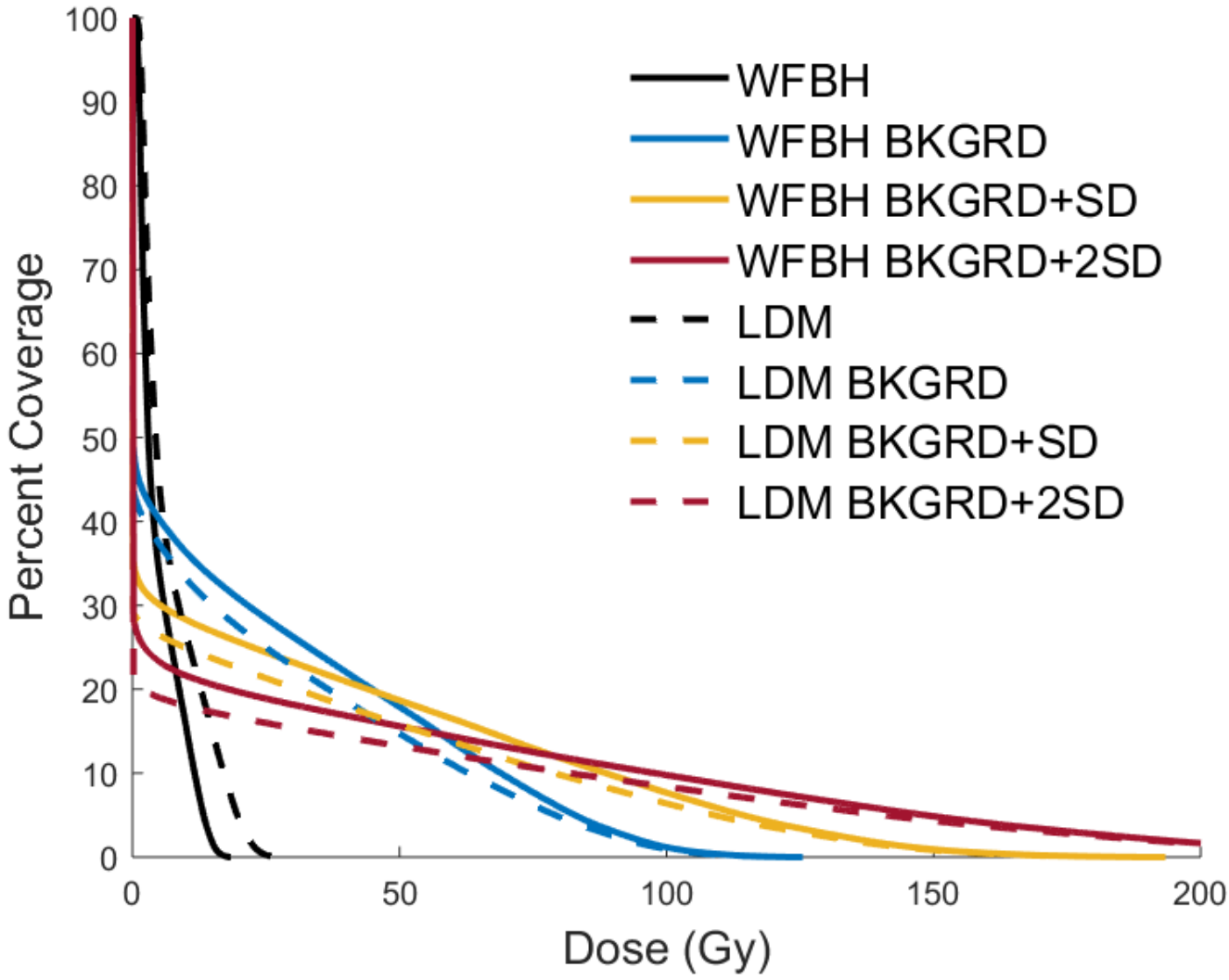

Figure 6

exampled of statistically different DVH curves We found that in a majority of cases these DVH curves between LDM and WFBH dose methods with and without background subtraction were not statistically different however this is an example of when this was not the case.

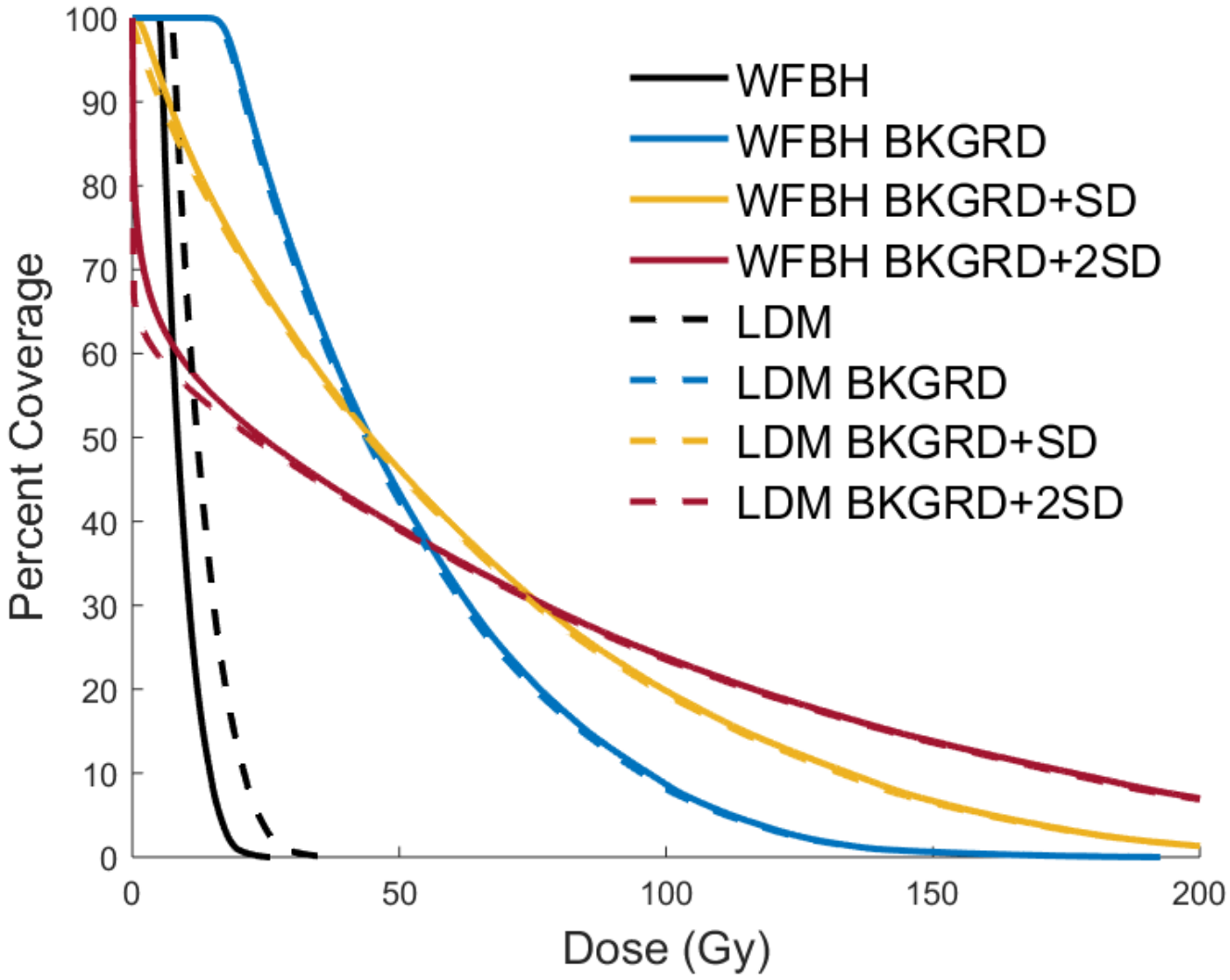

Figure 7

Treated region DVH curves Both dose calculation methods are effects by background subtraction in similar manners. As we increase the background subtraction value we see unrealistic distortion of the DVH curves.

Supplementary Files

This is a list of supplementary files associated with this preprint. Click to download.

- SupplementaryMaterialcode.pdf